Compressed Fourier-Domain Convolutional Beamforming for Sub-Nyquist Ultrasound Imaging

Alon Mamistvalov and Yonina C. Eldar, *Fellow, IEEE*

***Abstract*— Efficient ultrasound (US) systems that produce high-quality images can improve current clinical diagnosis capabilities by making the imaging process much more affordable and accessible to users. The most common technique for generating B-mode US images is delay-and-sum (DAS) beamforming, where an appropriate delay is introduced to signals sampled and processed at each transducer element. However, sampling rates that are much higher than the Nyquist rate of the signal are required for high-resolution DAS beamforming, leading to large amounts of data, making remote processing of channel data impractical. Moreover, the production of US images that exhibit high resolution and good image contrast requires a large set of transducer elements, which further increases the data size. Previous works suggest methods for reduction in sampling rate and in array size. In this work, we introduce compressed Fourier domain convolutional beamforming, combining Fourier domain beamforming (FDBF), sparse convolutional beamforming, and compressed sensing methods. This allows reducing both the number of array elements and the sampling rate in each element while achieving high-resolution images. Using *in vivo* data, we demonstrate that the proposed method can generate B-mode images using 142 times less data than DAS. Our results pave the way toward efficient US and demonstrate that high-resolution US images can be produced using sub-Nyquist sampling in time and space.**

***Index Terms*— Array processing, beamforming, compressed sensing (CS), medical ultrasound (US), sparse arrays.**

Nomenclature

M	Transducer array geometry.
$\|M\|$	Size of array M.
$\min(M), \max(M)$	Minimum and maximum element of array M.
$\boldsymbol{a}$	Vector.
$\boldsymbol{A}$	Matrix.
$*, *_s$	Discrete linear convolution over Fourier coefficients and discrete linear convolution over spatial dimension.
$\phi_m(t)$	Signal received at the mth transducer element.
$\hat{\phi}_m(t;\theta)$	Dynamically delayed received signal used for beamforming in direction θ.
$\Phi(t;\theta)$	Beamformed signal at direction θ.
$u_m(p;\theta)$	Normalized delayed signal at channel m.
T	Time duration of the receiving signal.
$c_m[k]$	kth Fourier coefficient of the received signal at channel m.
$c[k]$	kth Fourier coefficient of the beamformed signal.
$\hat{c}_m[k]$	kth Fourier coefficient of the delayed signal at channel m.
f_s	Sampling rate for traditional beamforming.
$N_{\text{st}} = \lfloor T \cdot f_s \rfloor$	Number of samples required for traditional beamforming.
β	Effective bandpass bandwidth of the received signal.
B	Cardinality of β.
$f_{sEN} = B/T$	Nyquist sampling rate of effective bandpass bandwidth of the received signal.
β_{sN}	Subset of β used for sub-Nyquist sampling.
B_{sN}	Cardinality of β_{sN}.
$N_{sN} = 2B_{sN} - 1$	Number of time samples corresponding to sub-Nyquist rate.

Manuscript received August 28, 2021; accepted October 22, 2021. Date of publication October 26, 2021; date of current version January 26, 2022. This work was supported in part by the Igel Manya Center for Biomedical Engineering and Signal Processing, in part by the Benoziyo Endowment Fund for the Advancement of Science, in part by the Estate of Olga Klein–Astrachan, and in part by the European Union's Horizon 2020 Research and Innovation Program under Grant 646804-ERC-COG-BNYQ. *(Corresponding author: Alon Mamistvalov.)*

The authors are with the Faculty of Mathematics and Computer Science, Weizmann Institute of Science, Rehovot 7610001, Israel (e-mail: alon.mamistvalov@weizmann.ac.il; yonina.eldar@weizmann.ac.il).

Digital Object Identifier 10.1109/TUFFC.2021.3123079

I. Introduction

ULTRASOUND (US) imaging is one of the most common medical imaging methods. It offers a wide range of noninvasive applications, including cardiac, fetal, and breast imaging. In traditional US, imaging is performed by transmit-

ting acoustic pulses along a narrow beam from an array of transducer elements. While propagating, echoes are scattered by acoustic impedance perturbations in the tissue and detected by the same array of transducers. The data collected by the receiving elements are then stored and processed to create an image line via beamforming [1]. In the process of beamforming, the signals are aligned by introducing appropriate time delays and subsequently averaged. Beamforming allows to focus and steer the beam to the desired direction corresponding to the transmission path or a point in space. This results in signal-to-noise ratio (SNR) improvement together with improved angular localization, which makes it one of the main components in the imaging cycle.

The standard approach for beamforming is delay-and-sum (DAS) beamforming [2], [3] due to its low computational cost and real-time capabilities. In DAS beamforming, delays are implemented digitally after sampling the signals in order to align the data, before averaging over the channels. To allow high-resolution time delays and avoid artifacts caused by the digital implementation of beamforming in time, US signals are typically sampled at a rate 4–10 times higher than their Nyquist rate [4].

To generate US images with high resolution and image contrast, the beam pattern of the beamformer should have narrow main lobe and low sidelobes [2], [5]. Although being simple for real-time applications, DAS suffers from low image resolution and contrast. Increasing the number of array elements can improve image quality when keeping the array pitch below half a wavelength to avoid grating sidelobes [6]. However, a large number of transducer elements, each sampling the signal at high rates, result in an enormous amount of data that need to be stored and processed, as well as many sampling channels. The large amount of data leads to impractical demands on the hardware and system power when considering portable devices and wireless probes. Therefore, rate reduction in time and space, together with image quality enhancement, is of great importance for portable US devices.

Several methods have been studied recently for data, power, and sampling rate reduction. Reduction in sampling rate has been investigated in several studies based on the combination of compressed sensing (CS) [7]–[10] and sub-Nyquist sampling [4] by exploiting the finite rate of innovation (FRI) [11] structure of the received US signal. It was shown in [8] and [9] that DAS beamforming can be implemented equivalently in the Fourier domain, leading to frequency-domain beamforming, with sampling rates lower than those known in today's commercial US systems. This was later extended to plane-wave imaging [12]. The suggested sub-Nyquist system was implemented in the context of radar [13] based on the ideas of Xampling presented in [7] and [14]–[17]. A CS-based synthetic transmit aperture technique is presented in [18]. This method increases the frame rate by transmitting a small number of randomly apodized plane waves and uses CS to recover the full channel data. However, none of the methods above considered the reduction in receiving elements.

Several approaches for generating US images using fewer receiving elements were studied in the literature. One example is relying on the analog implementation of subaperture and microbeamformers [19], where part of the beamformation is moved to the probe handle. However, this requires producing expensive integrated circuits with high power consumption and affects image quality [20]. Other methods considered the usage of sparse arrays [21]–[24] where some of the elements are removed. Cohen and Eldar [25] introduced a new beamforming method called convolutional beamforming algorithm (COBA). They showed that by applying COBA, the resulting beampattern is equivalent to that of the virtual array given by the sum coarray [26], [27]. Therefore, one can use thinned sparse arrays, whose sum coarray is a full uniform linear array (ULA), and obtain the same beampattern that would have been obtained using the original full array. Using COBA together with sparse economic array geometries can result in a large reduction of receiving elements, as shown in [25] and [28]–[34]. Although achieving reduction in the number of receiving elements, these techniques did not address lowering the sampling rate.

In [35], we presented the idea of combining both sampling rate reduction and spatial reduction. It was shown that US signals acquired by a sparse array can be subsampled to their effective Nyquist rate, delayed in the frequency domain, and then convolutionally beamformed, resulting in a US image with high image quality but produced from a small dataset. However, in [35], the structure of the convolutionally beamformed signal was not exploited to reduce the sampling rates to sub-Nyquist rates.

The main goal of this article is to present a beamforming and recovery method that reduces the number of receiving elements while sampling each of the channels at a rate lower than the Nyquist rate. We aim for a beamformer that preserves or improves image quality in terms of resolution and contrast when compared to DAS beamforming. To achieve this goal, we introduce a compressed frequency-domain convolutional beamforing algorithm (CFCOBA), which reconstructs the convolutionally beamformed signal from only a portion of the signal's Fourier coefficients and allows advanced imaging techniques such as harmonic imaging and coherent compounding [36].

We begin by introducing the relationship between the Fourier coefficients of the received signal to those of the convolutionally beamformed signal based on [9] and [25]. This relation uses the frequency equivalent of delaying signals in time and sparse arrays with desired sum coarray properties. We then show that the Fourier coefficients of the convolutionally beamformed signal can be calculated efficiently using the fast Fourier transform (FFT), making its implementation in real time possible. The proposed method for calculating the convolutionally beamformed signal Fourier coefficients requires only a portion of the signals' bandwidth and uses sparse arrays, resulting in massive data size reduction. To reconstruct the convolutionally beamformed signal, we prove that the signal obeys an FRI model based on the square of the known transmitted acoustic pulse, which enables recovery using known CS methods.

Next, we evaluate the suggested technique on simulated and *in vivo* data of several body parts scanned by different

US machines. Using this data, we show that US images can be produced without impacting image quality and even improving it when compared to DAS using up to two orders of magnitude less data. The data used for the proposed method are sampled at a rate lower than its effective Nyquist rate, which is typically much lower than its highest frequency. Thus, we illustrate that CFCOBA allows preservation of image quality with up to 142-fold reduction in data size due to the lower sampling rate and efficient sparse arrays used upon reception. Our approach offers significant data size reduction compared to common methods used today, combined with an efficient implementation, which can impact the system size, power consumption, cost, and mobility, making remote and wireless US imaging feasible.

The rest of this article is organized as follows. Section II discusses several beamforming methods such as DAS, Fourier domain beamforming, and COBA, together with examples of sparse arrays. Section III first presents our approach for combining data reduction in the acquiring array size and the sampling rate and then considers further reduction in sampling rate and reconstruction of the signal using CS methods. The performance of the suggested technique is evaluated in Section IV using phantom and *in vivo* scans. This article is concluded in Section V.

Nomenclature summarizes the notation used throughout this article.

II. Ultrasound Beamforming Techniques

In most US imaging systems, the US image is built line by line for each direction θ using multiple transducer elements to transmit and receive acoustic pulses. In that way, beamforming can be performed both during transmission and reception. We consider a ULA, M, comprised of $|M| = 2N - 1$ transducer elements aligned along the x-axis. The imaging cycle starts at $t = 0$ when the pulse is transmitted by each transducer element, resulting in a beam propagating at direction θ through the tissue. The energy is scattered by reflectors and the echoes are received by all elements at times that depend on their location.

Traditionally, US beamforming is performed for each imaging direction, θ, by averaging the received signals at different array elements while compensating for the differences in arrival time by alligning the signals using time shifts [8], [37]. This is referred to as DAS beamforming. In practice, DAS beamforming is performed digitally in the time domain. The applied delays are on the order of nanoseconds, which results in a sampling rate that can be as high as hundreds of megahertz [38], a requirement that is impractical. Therefore, US data signals are sampled at lower rates, on the order of tens of megahertz, and fine delay resolution is obtained by subsequent digital interpolation that adds an additional computational load. Yet, these lower rates are still typically much higher than the Nyquist rate of the signal that is twice its bandwidth [4] and often reach 4–10 times the transducer central frequency. These high sampling rates, together with the large number of array elements used, result in a huge amount of data, which makes the processing of US channel data inefficient and very difficult to do using portable devices.

A. Frequency-Domain Beamforming

To reduce the sampling rate, frequency-domain beamforming was suggested in [8] and [9]. Chernyakova *et al.* [9] showed the equivalence of performing beamforming in time and in the Fourier domain. It was then shown that beamforming can be performed efficiently using a small number of Fourier coefficients of the received signals, which translates to a low sampling rate. Specifically, let $c[k]$ denote the kth Fourier series coefficient of the beamformed signal and $c_m[k]$ the kth Fourier series coefficient of the received signal at channel m. Chernyakova *et al.* [9] showed that

$$c[k] = \frac{1}{|M|} \sum_{m=1}^{|M|} \sum_{n=-N_1}^{N_2} c_m[k-n] Q_{k,m;\theta}[n]. \tag{1}$$

Here, the variables $Q_{k,m;\theta}[n]$ are the Fourier coefficients of a distortion function that is determined solely by the geometry of the imaging setup and can be computed offline once and in advance. Using the Fourier coefficients of the distortion function, delaying is transferred to the frequency domain. The summation in (1) is actually infinite; however, in practice, it can be replaced by a relatively small finite summation due to the decay properties of $\{Q_{k,m;\theta}[n]\}$ and the fact that most of the energy of this set is centered around the dc component. Thus, $\{Q_{k,m;\theta}[n]\}$ decays rapidly for $n < -N_1$, $n > N_2$, where $N_1, N_2 \in \mathbb{N}$. Appropriate zero padding and applying an inverse Fourier transform (IFFT) to $\{c[k]\}$ results in the time-domain beamformed signal.

The importance of (1) is that it only requires the nonzero Fourier coefficients of the received signal. Those coefficients are obtained from sub-Nyquist samples of the signal at each receiving element. As shown in [9], the beamformed signal will contain at most $(B + N_1 + N_2)$ nonzero frequency components, where B is the cardinality of the set of ks for which $c_m[k]$ is nonzero. In practice, due to the fast decaying property of the distortion function, $B \gg N_1, N_2$ implies that the bandwidth of the beamformed signal equals B. Hence, to perform beamforming in frequency, we need only a portion of the Fourier coefficients of the signal. To obtain them, we use the Xampling mechanism proposed in [7]. The implementation of this mechanism is discussed in [13]. The output is sampled at its effective Nyquist rate and the required Fourier coefficients are the Fourier transform of the output. This yields a data size reduction of N_{st}/B, where N_{st} is the number of samples required for DAS beamforming.

B. Convolutional Beamforming

The Fourier domain beamforming (FDBF) method above focused on reducing sampling rate in time. An alternative method, COBA [25], [28], was suggested in order to reduce the number of array elements, assuming high sampling rate in time. COBA produces images, at least as good as those obtained by DAS, using fewer array elements. Here, we briefly present the COBA and propose a sparse array geometry that allows reduction in the number of elements.

Let $\hat{\phi}_m(p,\theta)$ denote the delayed signal at channel m, sampled at sampling intervals $T_s = (1/f_s)$, where f_s is the sampling rate used for traditional DAS and p stands for the pth sample. Cohen *et al.* [25] defined the beamformed signal in COBA as

$$\Phi_{\text{COBA}}(p;\theta) = \sum_{n=-(N-1)}^{N-1} \sum_{m=-(N-1)}^{N-1} u_n(p;\theta) u_m(p;\theta) \quad (2)$$

where

$$u_m(p;\theta) = e^{j\angle\hat{\phi}_m(p;\theta)} \sqrt{|\hat{\phi}_m(p;\theta)|} \quad (3)$$

with $\angle\hat{\phi}_m(p,\theta)$ and $|\hat{\phi}_m(p,\theta)|$ being the phase and the magnitude of $\hat{\phi}_m(p,\theta)$, respectively. The operation in (3), ensures that the amplitude of each product in (2) will be on the same order of the received signal at each channel.

The imaging characteristics in US, such as contrast and resolution, are determined by the beampattern of the beamformer. Specifically, a large number of elements ensure a narrow main lobe and low sidelobes, leading to high resolution and contrast. Hence, to analyze the imaging properties, the beampattern of the beamformer is often considered. To that end, in [25], it was shown that the effective beampattern of COBA is given by

$$H_{\text{COBA}}(\theta) = \sum_{n=-2(N-1)}^{2(N-1)} a_n \exp\left(-j\omega_0 \frac{\delta \sin\theta}{c} n\right) \quad (4)$$

where a_n are intrinsic apodization weights given by $\boldsymbol{a} = \mathbb{I}_M * \mathbb{I}_M$. Here, $\mathbb{I}_M$ is a binary vector whose mth entry is 1 if $m \in M$, ω_0 is the central frequency of the transducer, and $\delta_n = n\delta$, with δ being the distance between two consecutive array elements.

The key point from (4) is that the effective beampattern obtained by COBA is equivalent to the beampattern that would have been obtained using the sum coarray of the given physical array [26], [27], [39], which produces images with better resolution and contrast. The sum coarray is defined in Definition 1.

Definition 1 Sum Coarray): Consider a linear array M and define the set

$$\tilde{S}_M = \{n + m : n, m \in M\}. \quad (5)$$

The sumset S_M of the set M is defined to consist of the distinct elements of $\tilde{S}_M$. The array with elements located at $n\delta$ and $n \in S_M$ is the sum coarray of M.

The sum coarray is larger than the original array, which leads to improved imaging performance due to the effective beampattern. Therefore, a thinned array, comprised of the original array after removing some of its elements, can be used to actually reduce the data size. By preserving the desired sum coarray, the beampattern is not changed and might be improved.

Specific array geometries that were previously suggested include fractal arrays [28], [30]–[34], which were shown to generate a wide variety of good sparse arrays. Fractal arrays are defined recursively by

$$\begin{aligned} W_0 &= 0 \\ W_{r+1} &= \cup_{n\in\mathbb{G}}\left(W_r + nL^r\right), \quad r \in \mathbb{N} \end{aligned} \quad (6)$$

where the array $\mathbb{G}$ is the generator array in fractal terminology, with $\min(\mathbb{G}) = 0$. The translation factor L is given by $L = 2\max(\mathbb{G}) + 1$, where r is the array order. The resulting array, W, is composed of spatially arranged copies of $\mathbb{G}$. This choice leads to very thin arrays with desirable properties and coarrays that include the ULA of size $|M|$.

Using thinned arrays leads to reduction in power and data rates since less data are sampled, processed, and stored.

III. Compressed Frequency-Domain COBA

We now consider reconstruction of the convolutional beamformed signal from partial frequency data. We first show in Section III-A that FDBF can be combined with COBA [35], in order to sample at the Nyquist rate. Then, in Section III-B, we show that we can further reduce the rate in time leading to a method that allows to recover high-quality beamformed data from subsamples in both time and space.

A. Frequency-Domain COBA

We first show that FDBF can be combined with COBA [35]. This leads to an efficient beamforming method using a small number of array elements, each sampled at the effective Nyquist rate of the signal, without impacting the image quality compared to DAS.

Consider a ULA of desired aperture $|M|$ and a given array geometry $U \subseteq M$ corresponding to a desired array following Section II. The signal $\phi_m(t;\theta)$ is acquired by the receiving element m. Let $c_m[k]$ be the kth Fourier series coefficient of the received signal at channel m

$$c_m[k] = \frac{1}{T} \int 0^T I_{[0,T_B(\theta))}(t) \phi_m(t;\theta) e^{\frac{-2\pi j}{T} kt} dt. \quad (7)$$

As stated in [9], a typical US signal has one main band of energy, of bandwidth B. The energy outside this band is much lower, and hence, the sampling rate of the signal is set to achieve a consecutive set of the Fourier coefficients of the received signals, β, such that $|\beta| = B$. This implies that the sampling rate of the signal is dictated by the bandwidth of the signal and denoted by $f_{sEN} = B/T$, with T being the pulse penetration depth.

Next, as shown in (1), by multiplying the Fourier coefficients of the distortion function and the Fourier coefficients of the received signals elementwise, an appropriate delay is applied to the received signals, obtaining the Fourier coefficients of the delayed signal. The frequency-domain delayed (FDD) signal, $\hat{\phi}_m^{\text{FDD}}(p;\theta)$, is obtained by applying an IFFT on (1), before spatial domain summation. Here, p denotes the pth sample of the signal on the time grid of the delayed signal, $p = 1, \ldots, N_{\text{st}}$. By plugging $\hat{\phi}_m^{\text{FDD}}(p;\theta)$ into (3), we get

$$u_n^{\text{FDD}}(p;\theta) = u_n^{\text{TDD}}(p;\theta). \quad (8)$$

We refer to time domain delayed as TDD, which holds for a signal delayed using traditional time-domain delaying. The key idea is that the delay can be achieved regardless of the array geometry. Having obtained the equivalence of the

delayed signals in time and frequency, we can easily proceed in applying COBA.

Finally, we plug both the time domain and the FDD signals into (2) and proceed according to COBA as given in (2), which results in equivalence of the convolutional beamforming applied to TDD signal and FDD signal.

By combining COBA and FDBF, one can sample using a sparse set of array elements each sampled at the Nyquist rate of the signal. The resulting data size reduction is therefore $(|M|/|U|)(N_{\text{st}}/B)$, where $|M|$ and $|U|$ are the original and the thinned arrays size, respectively, N_{st} is the number of samples traditionally needed for DAS, and B is the actual signal bandwidth.

B. Exploiting the Fourier Coefficients Relationship

We now show how to further reduce the samlping in time without affecting image quality. To this end, we first derive a relation between the Fourier coefficients of the convolutionally beamformed signal and the Fourier coefficients of the received signals at the channels of U, the desired array geometry defined in Section II-B. Then, we examine the FRI structure of the convolutionally beamformed signal and prove that based on the FRI model, we can reconstruct the convolutionally beamformed signal from only a portion of its Fourier coefficients.

To obtain the desired relation, we describe several steps and the following calculation is performed for selected θ and for signals that correspond to FDD; those subscripts are not written explicitly for brevity. We aim to reduce the sampling rate further than proposed in [35], by obtaining a set of consecutive Fourier coefficients, $\beta_{sN} \subseteq \beta$. The set β_{sN} is acquired using an appropriate filter [7]

$$\phi_m(n_s) = \int_{-\infty}^{\infty} \phi_m(t) f_r(t - n_s T_{sN}) dt \tag{9}$$

where

$$f_r(t) = \sum_{l=-r}^{r} f(t + lT) \tag{10}$$

r is a constant determined by the support of the transmitted pulse, T is the duration of the received signals, and T_{sN} is the sampling period for sub-Nyquist sampling. The filter, $f(t)$, satisfies the following frequency response:

$$F(\omega) = \begin{cases} 0, & \text{if } \omega = \dfrac{2\pi k}{T}, \quad k \notin \beta_{sN} \\ 1, & \text{if } \omega = \dfrac{2\pi k}{T}, \quad k \in \beta_{sN} \\ \text{arbitrary}, & \text{else.} \end{cases} \tag{11}$$

Let N_{sN} be the number of samples acquired by sub-Nyquist sampling of the received signal. We define the compressed frequency-domain signal by

$$\hat{\Phi}(n_s)_{\text{CFCOBA}} = \sum_{n\in U} \sum_{m\in U} \hat{\phi}_n(n_s)\hat{\phi}_m(n_s) \tag{12}$$

where $n_s = 0, \ldots, N_{sN} - 1$ are the discrete time samples and $\hat{\phi}_m(n_s)$ and $\hat{\phi}_n(n_s)$ are the delayed signals at channels m and n, respectively, with the delay applied in the frequency domain. Each of the delayed signals has $B_{sN} = |\beta_{sN}|$ Fourier coefficients that are not zero, dictated by the filters width. The Fourier coefficients of the acquired signals are zero padded to length $N_{sN} = 2B_{sN} - 1$. Based on the multiplication in the time domain, the signal $\hat{\Phi}(n_s)_{\text{CFCOBA}}$ has $2B_{sN} - 1$ nonzero Fourier coefficients.

Next, we write the Fourier coefficients of the convolutionally beamformed signal based on the N_{sN} samples acquired

$$\hat{c}[k]_{\text{CFCOBA}} = \sum_{l\in U} \sum_{m\in U} \sum_{n_s=0}^{N_{sN}-1} \hat{\phi}_l(n_s)\hat{\phi}_m(n_s) \exp\left(\frac{-2\pi i}{N_{sN}} k n_s\right). \tag{13}$$

By plugging the Fourier series coefficients of the delayed signal at each channel, we have

$$\begin{aligned} \hat{c}[k]_{\text{CFCOBA}} &= \sum_{l\in U} \sum_{m\in U} \sum_{n_s=0}^{N_{sN}-1} \sum_{p=0}^{N_{sN}-1} \hat{c}_m[p] \exp\left(\frac{2\pi i}{N_{sN}} p n_s\right) \\ &\quad \sum_{q=0}^{N_{sN}-1} \hat{c}_l[q] \exp\left(\frac{2\pi i}{N_{sN}} q n_s\right) \exp\left(\frac{-2\pi i}{N_{sN}} k n_s\right) \end{aligned} \tag{14}$$

where the number of nonzero elements of $\{c_m[p]\}, \{c_l[q]\}$ is B_{sN}. Using the fact that

$$\sum_{n_s=0}^{N_{sN}-1} \exp\left(\frac{2\pi i}{N_{sN}}(p + q - k) n_s\right) = \begin{cases} N_{sN}, & \text{if } \; q + p = k \\ 0, & \text{else} \end{cases} \tag{15}$$

we get

$$\begin{aligned} \hat{c}[k]_{\text{CFCOBA}} &= N_{sN} \sum_{l\in U} \sum_{m\in U} \sum_{p+q=k} \hat{c}_m[p]\hat{c}_l[q] \\ &= N_s \sum_{l\in U} \sum_{m\in U} (\hat{c}_m * \hat{c}_l)[k] \end{aligned} \tag{16}$$

where the last equation is obtained by setting $q = k - p$. Hence, the resulting vector $\hat{c}[k]_{CFCOBA}$ has support size $2B_{sN} - 1 = N_{sN}$ and $k \in S_{\beta_{sN}}$, where $S_{\beta_{sN}}$ is the sumset of β_{sN} [26], [27].

Finally, plugging the Fourier coefficients of the delayed signal, in the frequency domain, into (16), we get the Fourier coefficients of the convolutionally beamformed signal

$$\begin{aligned} \hat{c}[k]_{\text{CFCOBA}} &= N_{sN} \sum_{l\in U} \sum_{m\in U} \\ &\left(\sum_{w=-N_1}^{N_2} c_m[k - w] Q_{k,m}[w] * \sum_{h=-N_1}^{N_2} c_l[k - h] Q_{k,l}[h] \right) \end{aligned} \tag{17}$$

where the length of the sequence $c_m[k - w]$ is N_{sN} with B_{sN} elements that are not zero. To efficiently calculate (17), we follow [25] noticing that (12) can be written as

$$\begin{aligned} \Phi_{\text{CFCOBA}}(n_s) &= \sum_{l\in S_U} \sum_{m,v\in U: m+v=l} u_m(n_s)u_v(n_s) \\ &= \sum_{l\in S_U} \Big(u(n_s) *_s u(n_s) \Big)_l \end{aligned} \tag{18}$$

where S_U is the sum coarray of U. Due to the linear operations in the temporal dimension that led to (17), we can plug the results into (18) leading to

$$\hat{c}[k]_{\text{CFCOBA}} = N_{sN} \sum_{l \in S_U} \left(\hat{c} \underset{s}{*} * \hat{c} \right)_l [k] \tag{19}$$

which denotes the 2-D convolution operation, one over the temporal dimension and one over the spatial dimension. This calculation can be easily calculated using IFFT and appropriate zero padding based on the convolution theorem, which leads to an efficient implementation with run time complexity of order $O(|U|N_{sN} \log(|U|N_{sN}))$.

The same derivation can be applied to the convolutionally beamformed signal, sampled at the traditional sampling rate for DAS beamforming. The signal is defined by

$$\hat{\Phi}(n_{\text{st}})_{\text{COBA}} = \sum_{n \in U} \sum_{m \in U} \hat{\phi}_n(n_{\text{st}}) \hat{\phi}_m(n_{\text{st}}) \tag{20}$$

where $n_{\text{st}} \in \{0, \ldots, N_{\text{st}} - 1\}$ is the n_{st}th sample of the delayed signal, and the signals are delayed in the frequency domain based on (1). In this case, the size of the set of the nonzero Fourier coefficients is $B \gg B_{sN}$ and $N_{\text{st}} \gg N_{sN}$. This results in

$$\hat{c}[k]_{\text{COBA}} = N_{\text{st}} \sum_{l \in U} \sum_{m \in U} \left(\sum_{w=-N_1}^{N_2} c_m[k-w] Q_{k,m}[w] * \sum_{h=-N_1}^{N_2} c_l[k-h] Q_{k,l}[h] \right) \tag{21}$$

where $\{c_m[k]\}_{k=0}^{N_{sN}-1} \subset \{c_m^{st}[k]\}_{k=0}^{N_{\text{st}}-1}$ and $c_m[k] = c_m^{\text{st}}[k]$, $\forall k \in \beta_{sN}$. The resulting subsampled signal Fourier coefficients thus satisfy

$$\hat{c}^{sN}[k]_{\text{CFCOBA}} = \hat{c}^{\text{st}}[k]_{\text{COBA}} \quad \forall k \in S_{\beta_{sN}}. \tag{22}$$

We next discuss reconstruction based on this partial set of Fourier coefficients.

C. FRI Structure Derivation

We first show that the convolutionally beamformed signal follows an FRI model.

Theorem 1: Let $\hat{\Phi}(t)_{\text{COBA}}$ be the convolutionally beadformed signal defined in (20) over continuous time. For any acquiring array, U, the convolutionally beamformed signal can be modeled as an FRI signal, i.e., it has the following structure:

$$\hat{\Phi}(t)_{\text{COBA}} = \sum_{s=1}^{S} b_s g(t - t_s) \tag{23}$$

where S is the number of scattering elements in the tissue in certain direction θ, $g(t) = h^2(t)$, where $h(t)$ is the transmitted pulse shape and $\{b_s\}$ and $\{t_s\}$ are the unknown amplitudes of the reflections and the times at which the reflection from the sth scatterer arrived at the receiving element, respectively.

Proof: From [8], we know that the delayed signal at each element has the form

$$\hat{\phi}_m(t) = \sum_{s=1}^{S} a_{s,m} h(t - t_s). \tag{24}$$

Substituting (24) into (20), we get

$$\Phi_{\text{COBA}}(t) = \sum_{l \in U} \sum_{m \in U} \left(\sum_{s=1}^{S} a_{s,l} h(t - t_s) \right) \left(\sum_{s'=1}^{S} a_{s',m} h(t - t_{s'}) \right). \tag{25}$$

Next, we assume that $h(t)$ is supported on a compact interval $[0, \Delta)$, $\Delta > 0$, meaning that $h(t - t_s)$ is supported on $[t_s, t_s + \Delta)$. We also assume that $t_s \gg \Delta$ so that in (25), all pairwise multiplications of $h(t - t_s)$ that involve $s \neq s'$ are zero. Thus, the beamformed signal is of the form

$$\begin{aligned} \Phi_{\text{COBA}}(t) &= \sum_{l \in U} \sum_{m \in U} \left(\sum_{s=1}^{S} a_{s,l} a_{s,m} h^2(t - s) \right) \\ &= \sum_{s=1}^{S} \left(\sum_{l \in U} \sum_{m \in U} a_{s,l} a_{s,m} \right) h^2(t - t_s) \\ &= \sum_{s=1}^{S} b_s g(t - t_s) \end{aligned} \tag{26}$$

where $g(t) = h^2(t)$. ■

Using the FRI structure of the convolutionally beamformed signal, we now address its reconstruction.

Corollary 1.1: Let $\{\hat{c}[k]_{\text{CFCOBA}}\}_{k \in S_{\beta_{sN}}}$ be the set of size $2B_{sN} - 1 > 2S$ nonzero consecutive Fourier coefficients of the CFCOBA signal defined in (12). Based on the FRI model, this signal can be recovered from a partial set of its Fourier coefficients by solving

$$\hat{\boldsymbol{c}}_{\boldsymbol{CFCOBA}} = \boldsymbol{GVb} \tag{27}$$

where $\hat{\boldsymbol{c}}_{\text{CFCOBA}}$ is a vector of size $2B_{sN} - 1$ with the nonzero $\{\hat{c}[k]_{\text{CFCOBA}}\}_{k \in S_{\beta_{sN}}}$ as its entries, $\boldsymbol{G}$ is a diagonal matrix of size $(2B_{sN} - 1) \times (2B_{sN} - 1)$ with $G(2\pi k/T)$ on its diagonal, $\boldsymbol{V}$ is a Fourier matrix of size $2B_{sN} - 1 \times S$ with (k, s)th element $e^{-j((2\pi)/T)kt_s}$, and $\boldsymbol{b}$ is the S-length vector with the amplitudes, $\{b_s\}$, as its entries.

Proof: We begin by noticing that the signal is completely defined by $2S$ unknown parameters that are the amplitudes $\{b_s\}$ and the delays $\{t_s\}$. For a duration T, the Fourier series expansion of (26) can be written as

$$\begin{aligned} \hat{c}[k]_{\text{CFCOBA}} &= \frac{1}{T} \int_0^T \sum_{s=1}^{S} b_s g(t - t_s) e^{-j((2\pi)/T)kt} dt \\ &= G\left(\frac{2\pi k}{T} \right) \sum_{s=1}^{S} b_s e^{-j((2\pi)/T)kt_s} \end{aligned} \tag{28}$$

where $\hat{c}[k]_{\text{CFCOBA}}$ are the Fourier coefficients of the convolutionally beamformed signal and $G(\omega)$ is the continuous time Fourier transform of $g(t)$. Writing (28) in matrix form results in (27). This problem is invertible as long as $2B_{sN} - 1 > S$ and the time delays $t_s \neq t_{s'}$, $\forall s \neq s'$. The formulation in (27) is a standard spectral analysis problem and can be solved for

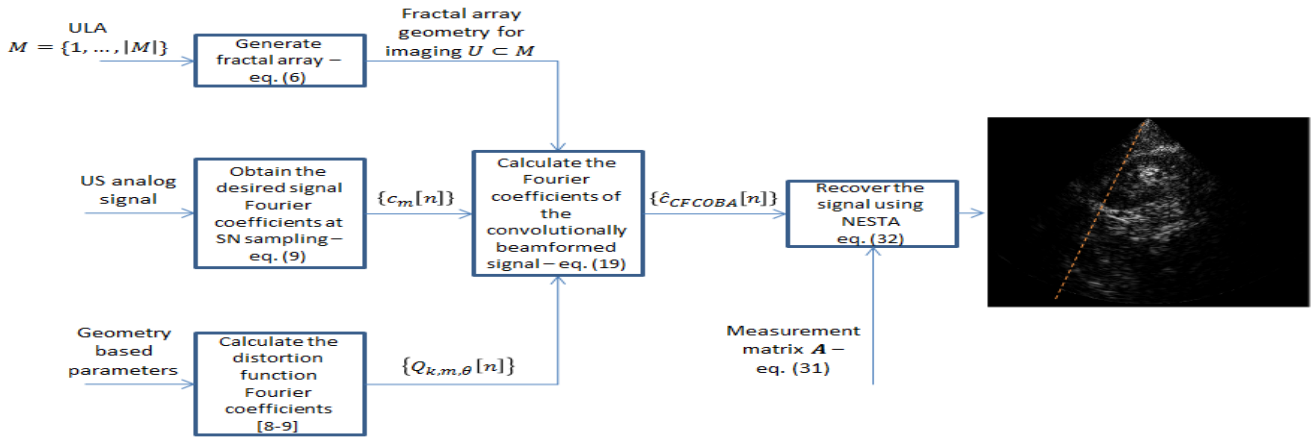

Fig. 1. CFCOBA algorithm and implementation flow. The basic steps include acquisition using a sparse array (6) and low rate sampling the signal (11). Using the geometry-based precalculated distortion function [8], [12], obtaining the convolutionally beamformed Fourier series coefficients (19). Finally, recovering the signal by solving the l_1 optimization problem with NESTA (32), using the appropriate measurement (31).

the unknown parameters $\{t_s, b_s\}_{s=1}^{S}$, using methods such as the annihilating filter [40]. ■

In practice, the recovery problem can be solved using CS methods as will be discussed next.

D. Reconstruction Using CS

To address recovery using CS methods, we begin with (28). By quantizing the delays with step $T_s = (1/f_s)$, such that $t_s = q_s T_s$, and letting $N_{\text{st}} = \lfloor T/T_s \rfloor$, the Fourier coefficients can be written as

$$\hat{c}[k]_{\text{CFCOBA}} = G\left(\frac{2\pi k}{T}\right) \sum_{s=0}^{N_{\text{st}}-1} \tilde{b}_s e^{-j((2\pi)/N_{\text{st}})ks}. \tag{29}$$

We define the vector $\tilde{\boldsymbol{b}}$ of length N_{st} to consist of

$$\tilde{b}_s = \begin{cases} b_s, & \text{if} \quad s = q_s \\ 0, & \text{else.} \end{cases} \tag{30}$$

The recovery problem then reduces to determining the S-sparse vector $\tilde{\boldsymbol{b}}$ from

$$\hat{c}_{\text{CFCOBA}} = \boldsymbol{G}\boldsymbol{D}\tilde{\boldsymbol{b}} = \boldsymbol{A}\tilde{\boldsymbol{b}} \tag{31}$$

where $\boldsymbol{D}$ is a $(2B_{sN}-1) \times N_{\text{st}}$ matrix, formed by taking the set $S_{\beta_{sN}}$ of rows from an $N_{\text{st}} \times N_{\text{st}}$ FFT matrix. This formulation is a classic CS problem and can be solved using many CS techniques. Choosing $N_{sN} \geq \text{CL}(\log N_{\text{st}})^4$ rows uniformly at random for some constant $C > 0$, the matrix $\boldsymbol{A}$ obeys the RIP with high probability [41].

In practice, due to speckle, the coefficient vector $\boldsymbol{b}$, defined in (30), is only approximately sparse. To reconstruct $\boldsymbol{b}$, we use the l_1 norm, leading to

$$\min_{\tilde{b}} ||\tilde{\boldsymbol{b}}||_1 \quad \text{s.t } ||\boldsymbol{A}\tilde{\boldsymbol{b}} - \hat{\boldsymbol{c}}_{\boldsymbol{CFCOBA}}||_2 \leq \epsilon \tag{32}$$

with ϵ being an appropriate noise level. This optimization problem can be solved using various known techniques, such as interior-point methods [42] or iterative shrinkage ideas [43], [44]. This optimization problem results in reconstruction of both strong and weak reflectors, as will be shown next through various examples.

A high-level flow and suggested implementation of the proposed method is shown in Fig. 1, for a specific image line.

IV. Evaluation Results

We now demonstrate the performance of the proposed beamforming algorithm in comparison to DAS and the non-compressed version of Fourier domain COBA. The methods are applied to point scatters simulated data, tissue-mimicking phantoms Gammex 403GSLE and 404GSLE, and RF data acquired from healthy volunteers. For verifying the wide variety of possible usages, we tested the methods on different datasets, each of different body parts. We present here *in vivo* cardiac data, kidney data, liver data, and bladder data. The proposed method is also quantitatively evaluated and compared to standard DAS in terms of contrast and image resolutions.

For evaluating axial and lateral resolution, full-width at half-maximum (FWHM) is calculated for *in vivo* data and phantom scans. The contrast ratio (CR) [25], [45] is calculated for contrast evaluation. CR is evaluated from two regions in each image: the cyst mimicking part and its background. The value is calculated prior to log compression, and it is obtained using

$$\text{CR} = 20\log_{10}\left(\frac{\mu_c}{\mu_b}\right) \tag{33}$$

where μ_b and μ_c denote the means of the background and the cyst, respectively.

Acquisition was performed using the GE breadboard ultrasonic scanner and the Verasonics Vantage 256 system. The scans made with the GE US machine were performed using 64 channels phased array probe, with a radiated depth of 16 cm. The probe carrier frequency was 3.4 MHz and the sampling rate was 16 MHz leading to 3328 samples per image line. The scans made with the Verasonics US machine were done using the 64-element phased array transducer P4-2v, with frequency response centered at 2.72 MHz and a sampling rate of 10.8 MHz. For the Verasonics setup, 1920 samples per image line were used. The simulated data were obtained using

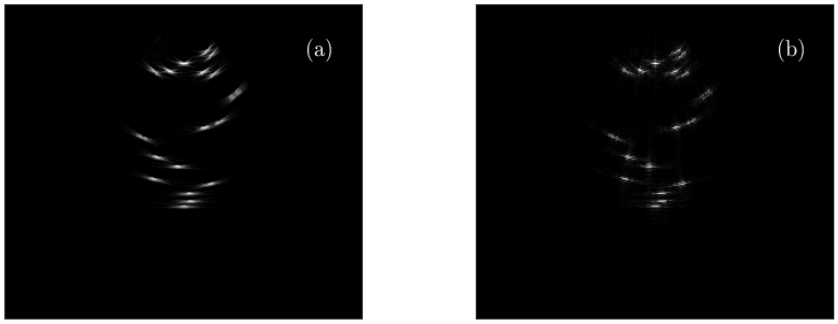

Fig. 2. Point scatterers simulated images obtained with (a) DAS and (b) compressed frequency-domain COBA—fractal geometry (36-fold reduction).

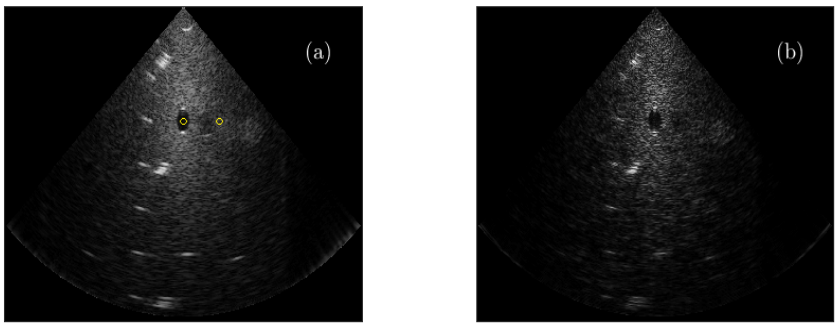

Fig. 3. Anechoic cyst phantom images obtained with (a) DAS and (b) compressed frequency-domain COBA—fractal geometry (36-fold reduction).

the Verasonics simulator based on the same setup used for the *in vivo* scans. The images were generated using standard steps, including log compression and interpolation.

For the fractal array geometry, we used the generator array $\mathbb{G} = \{0, 1\}$ and array order 4, leading to 15 elements. To perform beamforming in frequency, with the GE imaging setup, we used 400 and 100 samples at each of the channels of the fractal array geometry, leading to noncompressed and compressed frequency COBA images, respectively. This implies a 142-fold reduction in data size. For the Verasonics machine 480, 230 samples were used to perform noncompressed and compressed imaging using the sparse arrays leading to a reduction as high as 36 times less data. To solve (32), we used the Nesterov's algorithm (NESTA) [46], [47].

Table I shows a quantitative evaluation of the lateral and axial resolution of the compared reconstruction methods. The resolution is calculated from the *in vivo* scans and averaged over the four organs and for phantom scan data. The results were estimated by computing FWHM for each possible lateral and axial cut per frame and averaging the results over the total number of possible cuts per frame, i.e., for each image, the average resolution was calculated for both axial and lateral cuts, therefore presenting a reliable measure of the total image resolution without any preference to a specific direction. As can be seen, the resolution for the suggested method is comparable and effectively the same such as DAS resolution. The result makes sense due to the chosen fractal array geometry, which after CFCOBA yields the same effective array characteristics as described in Sections II-B and III-B.

Quantitative evaluation of CR is performed for the tissue-mimicking phantom using (33). The regions for calculating the contrast ratio are shown in Fig. 3. The CR of DAS and CFCOBA is -5.9 and -25 dB, respectively. These results indicate that CFCOBA is comparable to DAS and outperforms it in terms of image contrast, using much fewer array elements and samples for image formation.

Figs. 2 and 3 show the beamformed US images obtained from point scatterers simulation and phantom scans datasets. Figs. 2(a) and (b) and 3(a) and (b) show the standard DAS and the proposed beamforming method, CFCOBA, respectively. The resulting images clearly show that the proposed method outperforms standard methods for US imaging. It can be seen that in the point scatterers simulated data, the points are less blurred and the center of the reflector can be easily noticed. In the phantom setup scans, the strong reflectors are seen as good as in DAS images, and large noise reduction can be observed, i.e., the background "white noise" is much less observed emphasizing the contrast improvement.

The resulting *in vivo* US images are shown in Figs. 4–7. The images show four different frames of different body parts, where Figs. 4(a)–7(a) correspond to standard DAS, Figs. 4(b)–7(b) stand for COBA [25] with full ULA, Figs. 4(c)–7(c) stand for noncompressed Fourier domain COBA [35], and Figs. 4(d)–7(d) present the proposed compressed beamforming method. It can be easily seen that although the images are not identical, the resulting images, using compressed frequency-domain COBA, outperform those produced by standard DAS, not only in terms of image resolution and contrast but also in terms of image noise, using

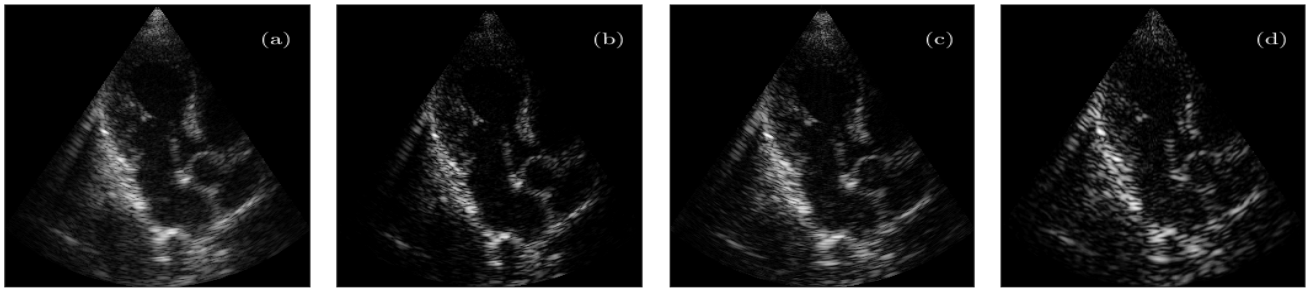

Fig. 4. GE US machine cardiac images obtained with (a) DAS, (b) COBA—full ULA, (c) Noncompressed frequency-domain COBA—fractal geometry (35-fold reduction), and (d) compressed frequency-domain COBA—fractal geometry (142-fold reduction).

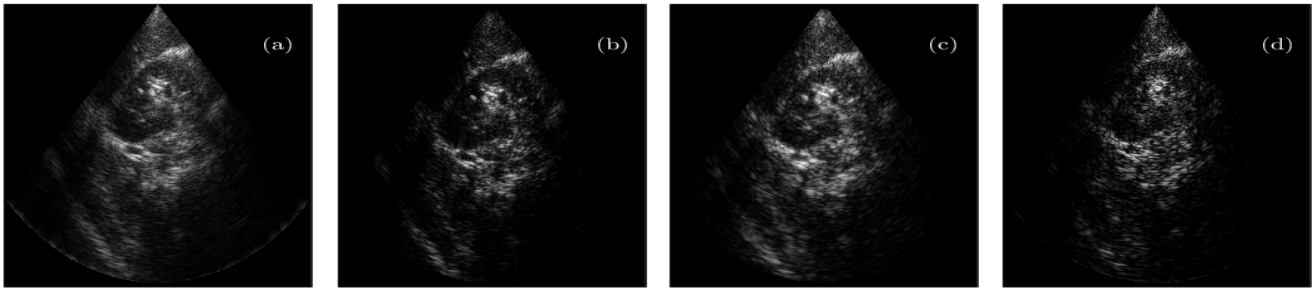

Fig. 5. Verasonics US machine kidney images obtained with (a) DAS, (b) COBA—full ULA, (c) noncompressed frequency-domain COBA—fractal geometry (17-fold reduction), and (d) compressed frequency-domain COBA—fractal geometry (36-fold reduction).

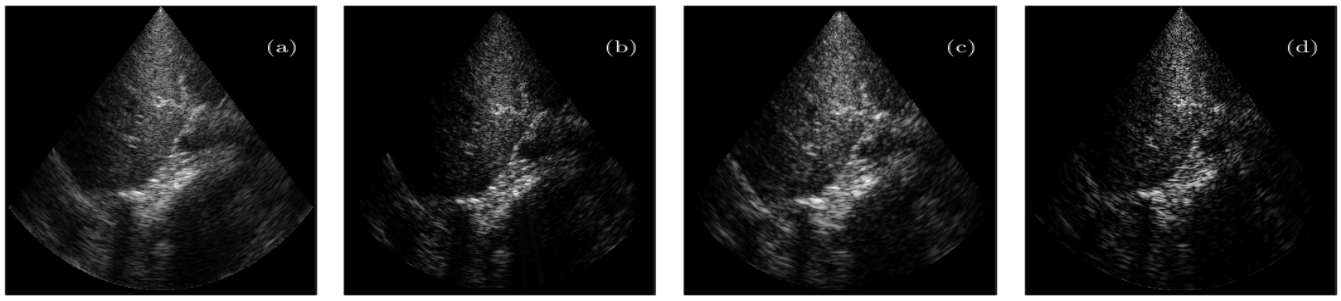

Fig. 6. Verasonics US machine liver images obtained with (a) DAS, (b) COBA—full ULA, (c) noncompressed frequency-domain COBA—fractal geometry (17-fold reduction), and (d) compressed frequency-domain COBA—fractal geometry (36-fold reduction).

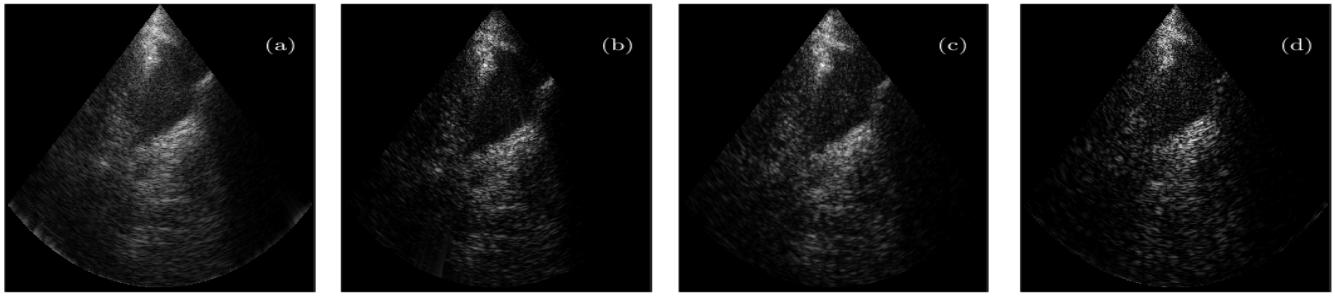

Fig. 7. Verasonics US machine bladder images obtained with (a) DAS, (b) COBA—full ULA, (c) noncompressed frequency-domain COBA—fractal geometry (17-fold reduction), and (d) compressed frequency-domain COBA—fractal COBA geometry (36-fold reduction).

two orders of magnitude less data. When comparing the results to the former proposed method, noncompressed FDBF, the outcome images do not differ much.

We now compute the computational complexity of CFCOBA and compare it to DAS. The common technique to performing DAS uses a linear interpolation of the time samples, according to the delay that should be applied, the computational complexity for this kind of interpolation is $O(N)$, for a given input of size N. In our case, $N = N_{\text{st}}$ and the interpolation is performed for all acquiring elements

TABLE I
RESOLUTION EVALUATION

Beamforming method	*in-vivo* data		Phantom data	
	axial	lateral	axial	lateral
DAS	3.68	4.92	3.2	4.5
CFCOBA	3.7	4.52	3.6	4.6

TABLE II
COMPUTATIONAL COMPLEXITY

Beamforming method	Experiment 1	Experiment 2
DAS	2×10^5	1.3×10^5
CFCOBA	2×10^4	8×10^4

to obtain one line of the image; therefore, the total number of operations for DAS is given by $|M| \times N_{\text{st}}$. In CFCOBA, the total number of operations is given by $|U|N_{sN}(\log(N_{sN}) + \log(|U|))$ for calculating the Fourier coefficients of the signal using 2-D FFT. For the recovery using the CS method, the complexity is given by N_{sN}^2 per image line, and hence, the total number of operations is given by $|U|N_{sN}(\log(N_{sN}) + \log(|U|) + N_{sN}^2$. Table II shows the comparison of the two methods for image recovery for the two setups we used, i.e., using the GE US machine, experiment 1, and the Verasonics setup, experiment 2, as can be seen in both setups, the suggested method outperforms DAS in terms of the estimated number of operations, resulting in order of magnitude fewer operations. For DAS, 64 receiving elements were used in both experiments, with 3328 samples for the GE setup and 1920 samples for the Verasonics setup. In CFCOBA, we used the fractal array geometry resulting in 15 receiving elements for both setups, using 100 samples in the GE experiment and 230 samples for the Verasonics.

These results combined with the quantitative results validate that a significant reduction in both the number of acquiring elements and the sampling rate can be achieved using the proposed technique without degrading image quality and even improving it when compared to traditional DAS using an efficient method.

V. CONCLUSION

In this article, we proposed a new beamforming method for high-quality B-mode US images. The suggested technique is based on Xampling, frequency-domain beamforming, CS, sparse arrays, and convolutional beamforming all implemented efficiently. This combination allows producing a beamformer that can outperform the widely used DAS using fewer receive elements and data.

We extended frequency-domain COBA presented in [35] and showed that the COBA can be performed directly in the frequency domain. This results in up to 33-fold reduction in sampling rate and 142 times less data combining with sparse convolutional beamforming, without impacting image quality and even improving it. The huge reduction is achieved by sampling the signals at sub-Nyquist rates and using the Xampling mechanism. To reconstruct the signal from partial frequency data, we derived an FRI model for the convolutionally beamformed signal, which resulted in replicas of the square of the known transmitted pulse. This result enabled usage of CS recovery methods.

Finally, we validated our technique both on simulated data and on *in vivo* channel data of a variety of body parts, acquired by two different US machines, resulting in high-quality B-mode US images, using orders of magnitude less data.

Our results prove that the idea of compressed US imaging is feasible for practical use, leading to potential reduction in US cost, power consumption and size, and paving the way toward efficient US imaging.

ACKNOWLEDGMENT

The authors would like to thank Dr. Israel Aharony for voluntarily performing the scans, which provided the data for testing and evaluating the proposed method, and Sivan Grotas for fruitful discussions.

REFERENCES

[1] B. D. Van Veen and K. M. Buckley, "Beamforming: A versatile approach to spatial filtering," *IEEE ASSP Mag.*, vol. 5, no. 2, pp. 4–24, Apr. 1988.
[2] K. E. Thomenius, "Evolution of ultrasound beamformers," in *Proc. IEEE Ultrason. Symp.*, vol. 2, Nov. 1996, pp. 1615–1622.
[3] B. D. Steinberg, "Digital beamforming in ultrasound," *IEEE Trans. Ultrason., Ferroelectr., Freq. Control*, vol. 39, no. 6, pp. 716–721, Nov. 1992.
[4] Y. C. Eldar, *Sampling Theory: Beyond Bandlimited Systems*. Cambridge, U.K.: Cambridge Univ. Press, 2015.
[5] K. Ranganathan and W. F. Walker, "A novel beamformer design method for medical ultrasound. Part I: Theory," *IEEE Trans. Ultrason., Ferroelectr., Freq. Control*, vol. 50, no. 1, pp. 15–24, Jan. 2003.
[6] G. R. Lockwood, J. R. Talman, and S. S. Brunke, "Real-time 3-D ultrasound imaging using sparse synthetic aperture beamforming," *IEEE Trans. Ultrason., Ferroelectr., Freq. Control*, vol. 45, no. 4, pp. 980–988, Jul. 1998.
[7] R. Tur, Y. C. Eldar, and Z. Friedman, "Innovation rate sampling of pulse streams with application to ultrasound imaging," *IEEE Trans. Signal Process.*, vol. 59, no. 4, pp. 1827–1842, Apr. 2011.
[8] N. Wagner, Y. C. Eldar, and Z. Friedman, "Compressed beamforming in ultrasound imaging," *IEEE Trans. Signal Process.*, vol. 60, no. 9, pp. 4643–4657, Sep. 2012.
[9] T. Chernyakova and Y. Eldar, "Fourier-domain beamforming: The path to compressed ultrasound imaging," *IEEE Trans. Ultrason., Ferroelectr., Freq. Control*, vol. 61, no. 8, pp. 1252–1267, Aug. 2014.
[10] Y. C. Eldar and G. Kutyniok, *Compressed Sensing: Theory and Applications*. Cambridge, U.K.: Cambridge Univ. Press, 2012.
[11] M. Vetterli, P. Marziliano, and T. Blu, "Sampling signals with finite rate of innovation," *IEEE Trans. Signal Process.*, vol. 50, no. 6, pp. 1417–1428, Jun. 2002.
[12] T. Chernyakova *et al.*, "Fourier-domain beamforming and structure-based reconstruction for plane-wave imaging," *IEEE Trans. Ultrason., Ferroelectr., Freq. Control*, vol. 65, no. 10, pp. 1810–1821, Oct. 2018.
[13] E. Baransky, G. Itzhak, N. Wagner, I. Shmuel, E. Shoshan, and Y. Eldar, "Sub-Nyquist radar prototype: Hardware and algorithm," *IEEE Trans. Aerosp. Electron. Syst.*, vol. 50, no. 2, pp. 809–822, Apr. 2014.
[14] T. Michaeli and Y. C. Eldar, "Xampling at the rate of innovation," *IEEE Trans. Signal Process.*, vol. 60, no. 3, pp. 1121–1133, Dec. 2011.
[15] M. Mishali, Y. C. Eldar, O. Dounaevsky, and E. Shoshan, "Xampling: Analog to digital at sub-Nyquist rates," *IET Circuits, Devices Syst.*, vol. 5, no. 1, pp. 8–20, Jan. 2011.
[16] M. Mishali, Y. C. Eldar, and A. J. Elron, "Xampling: Signal acquisition and processing in union of subspaces," *IEEE Trans. Signal Process.*, vol. 59, no. 10, pp. 4719–4734, Oct. 2011.
[17] K. Gedalyahu, R. Tur, and Y. C. Eldar, "Multichannel sampling of pulse streams at the rate of innovation," *IEEE Trans. Signal Process.*, vol. 59, no. 4, pp. 1491–1504, Apr. 2011.
[18] J. Liu, Q. He, and J. Luo, "A compressed sensing strategy for synthetic transmit aperture ultrasound imaging," *IEEE Trans. Med. Imag.*, vol. 36, no. 4, pp. 878–891, Apr. 2017.

[19] J. D. Larson III, "2-D phased array ultrasound imaging system with distributed phasing," U.S. Patent 5 229 933, Jul. 20, 1993.
[20] B. Savord and R. Solomon, "Fully sampled matrix transducer for real time 3D ultrasonic imaging," in *Proc. IEEE Symp. Ultrason.*, vol. 1, Oct. 2003, pp. 945–953.
[21] E. Roux *et al.*, "Validation of optimal 2D sparse arrays in focused mode: Phantom experiments," in *Proc. IEEE Int. Ultrason. Symp. (IUS)*, Sep. 2017, pp. 1–4.
[22] J. T. Yen, J. P. Steinberg, and S. W. Smith, "Sparse 2-D array design for real time rectilinear volumetric imaging," *IEEE Trans. Ultrason., Ferroelectr., Freq. Control*, vol. 47, no. 1, pp. 93–110, Jan. 2000.
[23] A. Austeng and S. Holm, "Sparse 2-D arrays for 3-D phased array imaging-design methods," *IEEE Trans. Ultrason., Ferroelectr., Freq. Control*, vol. 49, no. 8, pp. 1073–1086, Aug. 2002.
[24] S. S. Brunke and G. R. Lockwood, "Broad-bandwidth radiation patterns of sparse two-dimensional Vernier arrays," *IEEE Trans. Ultrason., Ferroelectr., Freq. control*, vol. 44, no. 5, pp. 1101–1109, Sep. 1997.
[25] R. Cohen and Y. C. Eldar, "Sparse convolutional beamforming for ultrasound imaging," *IEEE Trans. Ultrason., Ferroelectr., Freq. Control*, vol. 65, no. 12, pp. 2390–2406, Dec. 2018.
[26] C.-L. Liu and P. P. Vaidyanathan, "Maximally economic sparse arrays and Cantor arrays," in *Proc. IEEE 7th Int. Workshop Comput. Adv. Multi-Sensor Adapt. Process. (CAMSAP)*, Dec. 2017, pp. 1–5.
[27] R. Cohen and Y. C. Eldar, "Optimized sparse array design based on the sum coarray," in *Proc. IEEE Int. Conf. Acoust., Speech Signal Process. (ICASSP)*, Apr. 2018, pp. 3340–3343.
[28] R. Cohen and Y. C. Eldar, "Sparse array design via fractal geometries," *IEEE Trans. Signal Process.*, vol. 68, pp. 4797–4812, 2020.
[29] R. Cohen and Y. C. Eldar, "Sparse fractal array design with increased degrees of freedom," in *Proc. IEEE Int. Conf. Acoust., Speech Signal Process. (ICASSP)*, May 2019, pp. 4195–4199.
[30] C. Puente-Baliarda and R. Pous, "Fractal design of multiband and low side-lobe arrays," *IEEE Trans. Antennas Propag.*, vol. 44, no. 5, p. 730, May 1996.
[31] D. H. Werner, R. L. Haupt, and P. L. Werner, "Fractal antenna engineering: The theory and design of fractal antenna arrays," *IEEE Antennas Propag. Mag.*, vol. 41, no. 5, pp. 37–58, Oct. 1999.
[32] D. H. Werner and S. Ganguly, "An overview of fractal antenna engineering research," *IEEE Antennas Propag. Mag.*, vol. 45, no. 1, pp. 38–57, Feb. 2003.
[33] J. Feder, *Fractals*. Berlin, Germany: Springer, 2013.
[34] K. Falconer, *Fractal Geometry: Mathematical Foundations and Applications*. Hoboken, NJ, USA: Wiley, 2004.
[35] A. Mamistvalov and Y. C. Eldar, "Sparse convolutional beamforming for wireless ultrasound," in *Proc. IEEE Int. Conf. Acoust., Speech Signal Process. (ICASSP)*, May 2020, pp. 9254–9258.
[36] R. Cohen, N. Fingerhut, F. Varray, H. Liebgott, and Y. C. Eldar, "Sparse convolutional beamforming for 3-D ultrafast ultrasound imaging," *IEEE Trans. Ultrason., Ferroelectr., Freq. Control*, vol. 68, no. 7, pp. 2444–2459, Jul. 2021.
[37] J. A. Jensen, "Linear description of ultrasound imaging systems: Notes for the international summer school on advanced ultrasound imaging at the technical university of Denmark," Tech. Univ. Denmark, Lyngby, Denmark, Tech. Rep., Jul. 1999.
[38] G. DeMuth, "Frequency domain beamforming techniques," in *Proc. IEEE Int. Conf. Acoust., Speech, Signal Process. (ICASSP)*, vol. 2, May 1977, pp. 713–715.
[39] R. T. Hoctor and S. A. Kassam, "The unifying role of the coarray in aperture synthesis for coherent and incoherent imaging," *Proc. IEEE*, vol. 78, no. 4, pp. 735–752, Apr. 1990.
[40] P. Stoica, *Introduction to Spectral Analysis*. Upper Saddle River, NJ, USA: Prentice-Hall, 2000.
[41] M. Rudelson and R. Vershynin, "On sparse reconstruction from Fourier and Gaussian measurements," *Commun. Pure Appl. Math.*, vol. 61, no. 8, pp. 1025–1045, 2008.
[42] E. Cands and J. Romberg, "ℓ_1-magic: Recovery of sparse signals via complex programming," California Inst. Technol., Pasadena, CA, USA, Tech. Rep., 2005. [Online]. Available: https://www.acm.caltech.edu/l1magic/downloads/l1magic
[43] A. Beck and M. Teboulle, "A fast iterative shrinkage-thresholding algorithm for linear inverse problems," *SIAM J. Imag. Sci.*, vol. 2, no. 1, pp. 183–202, 2009.
[44] E. T. Hale, W. Yin, and Y. Zhang, "A fixed-point continuation method for ℓ_1-regularized minimization with applications to compressed sensing," Rice Univ., Houston, TX, USA, Tech. Rep. CAAM TR07-07, 2007, vol. 43, p. 44.
[45] J. J. Dahl, D. Hyun, M. Lediju, and G. E. Trahey, "Lesion detectability in diagnostic ultrasound with short-lag spatial coherence imaging," *Ultrason. Imag.*, vol. 33, no. 2, pp. 119–133, Apr. 2011.
[46] Y. Nesterov, "Smooth minimization of non-smooth functions," *Math. Program.*, vol. 103, no. 1, pp. 127–152, 2005.
[47] S. Becker, J. Bobin, and E. J. Candès, "NESTA: A fast and accurate first-order method for sparse recovery," *SIAM J. Imag. Sci.*, vol. 4, no. 1, pp. 1–39, 2011.

Alon Mamistvalov received the B.Sc. degree in physics and the B.Sc. degree in electrical engineering from the Technion–Israel Institute of Technology, Haifa, Israel, in 2017. He is currently pursuing the M.Sc. degree in mathematics and computer science with the Weizmann Institute of Science, Rehovot, Israel.

His research interests include signal processing, medical imaging, advanced signal processing methods for ultrasonic imaging, and deep learning for ultrasound imaging.

Yonina C. Eldar (Fellow, IEEE) received the B.Sc. degree in physics and the B.Sc. degree in electrical engineering from Tel Aviv University (TAU), Tel Aviv, Israel, in 1995 and 1996, respectively, and the Ph.D. degree in electrical engineering and computer science from the Massachusetts Institute of Technology (MIT), Cambridge, MA, USA, in 2002.

She was a Professor with the Department of Electrical Engineering, Technion–Israel Institute of Technology, Haifa, Israel, where she held the Edwards Chair in Engineering. She was a Visiting Professor at Stanford University, Stanford, CA, USA. She is currently a Professor with the Department of Mathematics and Computer Science, Weizmann Institute of Science, Rehovot, Israel. She is also a Visiting Professor with the Massachusetts Institute of Technology (MIT), Cambridge, MA, USA, a Visiting Scientist with the Broad Institute, MIT and Harvard, Cambridge, MA, USA, and an Adjunct Professor with Duke University, Durham, NC, USA. Her research interests include in the broad areas of statistical signal processing, sampling theory and compressed sensing, learning and optimization methods, and their applications to biology and optics.

Dr. Eldar was a member of the Young Israel Academy of Science and Humanities and the Israel Committee for Higher Education. She is a member of the Israel Academy of Sciences and Humanities (elected 2017) and a fellow of EURASIP. She has received many awards for excellence in research and teaching, including the IEEE Signal Processing Society Technical Achievement Award in 2013, the IEEE/AESS Fred Nathanson Memorial Radar Award in 2014, and the IEEE Kiyo Tomiyasu Award in 2016. She was a Horev Fellow of the Leaders in Science and Technology Program at the Technion and an Alon Fellow. She received the Michael Bruno Memorial Award from the Rothschild Foundation, the Weizmann Prize for Exact Sciences, the Wolf Foundation Krill Prize for Excellence in Scientific Research, the Henry Taub Prize for Excellence in Research (twice), the Hershel Rich Innovation Award (three times), the Award for Women with Distinguished Contributions, the Andre and Bella Meyer Lectureship, the Career Development Chair at the Technion, the Muriel and David Jacknow Award for Excellence in Teaching, and the Technion's Award for Excellence in Teaching (two times). She received several best paper awards and best demo awards together with her research students and colleagues, including the SIAM Outstanding Paper Prize, the UFFC Outstanding Paper Award, the Signal Processing Society Best Paper Award, and the *IET Circuits, Devices, and Systems* Premium Award. She was the co-chair and the technical co-chair of several international conferences and workshops. She was selected as one of the 50 most influential women in Israel. She is the Editor-in-Chief of *Foundations and Trends in Signal Processing* and a member of the IEEE Sensor Array and Multichannel Technical Committee. She serves on several other IEEE committees. In the past, she was a Signal Processing Society Distinguished Lecturer and a member of the IEEE Signal Processing Theory and Methods and Bio Imaging Signal Processing Technical Committees. She served as an Associate Editor for IEEE TRANSACTIONS ON SIGNAL PROCESSING, the *EURASIP Journal on Advances in Signal Processing*, the *SIAM Journal on Matrix Analysis and Applications*, and the *SIAM Journal on Imaging Sciences*.